ARCHIVE OF MECHANICAL ENGINEERING

VOL. LXII 2015 Number 2

10.1515/meceng-2015-0010

Key words: high velocity perforation, ductile fracture criteria, material tests, numerical simulations

DJALEL EDDINE TRIA [*], *RADOSŁAW TRĘBIŃSKI* [**]

ON THE INFLUENCE OF FRACTURE CRITERION ON PERFORATION OF HIGH-STRENGTH STEEL PLATES SUBJECTED TO ARMOUR PIERCING PROJECTILE

This paper presents a numerical investigation of fracture criterion influence on perforation of high-strength 30PM steel plates subjected to 7.62×51 mm Armour Piercing (AP) projectile. An evaluation of four ductile fracture models is performed to identify the most suitable fracture criterion. Included in the paper is the Modified Johnson-Cook (MJC) constitutive model coupled separately with one of these fracture criteria: the MJC fracture model, the Cockcroft-Latham (CL), the maximum shear stress and the constant failure strain models. A 3D explicit Lagrangian algorithm that includes both elements and particles, is used in this study to automatically convert distorted elements into meshless particles during the course of the computation. Numerical simulations are examined by comparing with the experimental results. The MJC fracture model formulated in the space of the stress triaxiality and the equivalent plastic strain to fracture were found capable of predicting the realistic fracture patterns and at the same time the correct projectile residual velocities. However, this study has shown that CL one parameter fracture criterion where only one simple material test is required for calibration is found to give good results as the MJC failure criterion. The maximum shear stress fracture criterion fails to capture the shear plugging failure and material fracture properties cannot be fully characterized with the constant fracture strain.

1. Introduction

Steel structures subjected to ballistic perforation are highly affected by large strains, high strain rates, thermal softening, varying stress states and loading history, which finally leads to failure [1-4]. It is therefore important to model the mechanical response of the impacted steel structure where all these

[*] *Department of Ballistics, Military University of Technology, ul. Gen. Kaliskiego 2, 00-902 Warsaw, Poland; Email: dtria@wat.edu.pl*

[**] *Department of Ballistics, Military University of Technology, ul. Gen. Kaliskiego 2, 00-902 Warsaw, Poland; Email: rkt@wat.edu.pl*

effects are accounted, and a material model will not be complete without the description of material degradation and failure.

In reality, since empirical and analytical approaches cannot capture all of the multiple physical phenomena including fracture, failure, residual stresses and friction heating, numerical simulation has become a necessary tool for the ballistic penetration study [5, 6].

A review of the literature on impact simulations shows that the most research in this field have been focused on the development and application of continuum hydro-codes using either mesh-based Lagrangian or mesh free formulations [7-12]. Lagrange formulation is widely used because of its low computational cost and the variety of complex material models and contact algorithms which are incorporated. However, it is very sensitive to mesh distortion which leads to time steps drop and error propagation. Numerical codes can handle these problems with adaptive re-meshing algorithms or by the use of mesh free methods like Smooth Particle Hydrodynamic (SPH). On the other hand, the limited applicability of adaptive re-meshing algorithms to 3D models decreases the attractiveness. Moreover, the SPH suffers from a numerical instability in tension and consequently the regions subjected to large tension exhibit numerical fracture and artificial voids [7, 13]. It is possible thanks to hybrid elements to switch from Finite Elements to SPH using a certain criteria in order to couple the benefits of both types of elements. With this technique, the activation of the SPH particles happens once Finite Elements have reached a too high level of distortion to continue the simulation. The generated particles keep the same mechanical properties and mass of the eroded elements [14-16].

Ductile materials, such as metals, fail as a result of nucleation, growth and coalescence of microscopic voids that initiate at inclusions and second phase particles [17-19]. Thus, it depends highly on the stress triaxiality, which has been confirmed in many experimental studies (see e.g. [20]). Several fracture criteria based on this realization have been proposed in the literature [2, 21, 22], where some are more complex than others. While some criteria depend only on the triaxial stress state, others take also the effects of strain rate and temperature into account. Thus, due to simplicity, a constant effective plastic strain to fracture is widely used to simulate crack formation and growth when the stress triaxiality varies spatially and temporally in a narrow range [18, 23]. Also, in high velocity impact, shear stresses are mostly responsible for the formation and growth of through-thickness of crack [22].

Previous studies [3, 9, 10, 24-26] show that the Johnson-Cook (JC) constitutive relation and Johnson-Cook (JC) fracture criterion with five material parameters give reliable results of the perforation problem. However, for design purposes, it is crucial that the number of material tests in numerical

simulations is minimized, since it is both costly and ineffective to perform a number of material tests each time a new material is considered.

Hence, the main objective of this study is to investigate if it is reliable to use a 3D finite element code together with a simple and easily calibrated model such Cockcroft-Latham (CL), the maximum shear stress and the constant failure strain models to predict the penetration process and failure patterns. Experimental data used for the comparison with numerical modeling are taken from ballistic perforation tests performed in the Laboratory of Ballistics at Military University of Technology. High strength steel plates (30PM) are used at different thicknesses (3 mm, 6 mm and 8 mm), and these are subjected to the impact with 7.62×51 mm AP bullet at initial velocity of 835 m/s. Material tests were performed for armour steel to develop the described models while material data for the bullet hard core, jacket and sabot are taken from literature.

2. The material models

2.1. The constitutive relation

A slightly modified version of the Johnson-Cook constitutive relation is chosen for this study, based on traditional plasticity theory that reproduces several material responses observed in impact and penetration of metals. This computational model expresses the equivalent flow stress as a function of the equivalent plastic strain, strain rate and temperature as [3, 24]:

$$\sigma_{eq} = \left(A + B\varepsilon_{eq}^{n}\right)\left(1 + \dot{\varepsilon}_{eq}^{*}\right)^{C}\left(1 - T^{*m}\right) \tag{1}$$

where A, B, C, n and m are material constants, ε_{eq} is the effective plastic strain, $\dot{\varepsilon}_{eq}^{*}$ is the dimensionless plastic strain rate, $T^{*} = (T - T_{room})/(T_{melt} - T_{room})$ is the homologous temperature.

The first bracket in the model represents the strain hardening, the second describes the strain-rate sensitivity and the third represents the temperature softening. This implies that the strain hardening, strain-rate hardening and temperature softening are independent of each other, i.e. the different influences are uncoupled in this model. Thus, it is only necessary to perform material tests where these effects are studied separately in order to determine the material constants. The slight modification in comparison to the original JC model lies on the strain rate part of the equation where the parameter C was multiplied by the logarithm of the equivalent strain rate.

The rate of temperature increase is computed from the energy balance by assuming adiabatic conditions

$$\dot{T} = \chi \frac{\sigma_{eq}\dot{\varepsilon}_{eq}}{\rho C_p} \tag{2}$$

where ρ is the material density, C_p is the specific heat and χ is the Taylor-Quinney coefficient that represents the proportion of plastic work converted into heat [24].

2.2. The fracture criteria

In many materials it is seen from experiments [2-4, 18] that failure strain increases with increasing temperature and may decrease with increasing strain rate, hence they both have an effect on the damage process during penetration. Johnson and Cook [2] made the failure strain ε_f dependent on strain path, strain rate and temperature, beside of being dependent on stress triaxiality. A slightly modified version of the original model, the MJC failure strain reads [24]

$$\varepsilon_f = (D_1 + D_2 \exp(D_3\sigma^*))\left(1 + \dot{\varepsilon_{eq}}^*\right)^{D_4}(1 + D_5 T^*) \tag{3}$$

where $D_1, \ldots, D_5$ are material constants determined from material tests, $\sigma^* = \dfrac{\sigma_H}{\sigma_{eq}}$ is the stress triaxiality ratio where σ_H is the hydrostatic stress.

The fracture criterion was based on damage evolution, where the damage of a material element is expressed as:

$$\dot{D} = \begin{cases} 0 & \text{for } \varepsilon_{eq} \le \varepsilon_d \\ \dfrac{D_c}{\varepsilon_f - \varepsilon_d}\dot{\varepsilon}_{eq} & \text{for } \varepsilon_{eq} > \varepsilon_d \end{cases} \tag{4}$$

where D_c is the critical damage and ε_d is a damage threshold. The failure is assumed to occur when D equals unity. For simplicity, the damage threshold parameter ε_d is taken equal to 0, while the critical damage D_c is taken equal to 1.0.

Alternatively, damage failure can be modeled using a fracture criterion proposed by Cockcroft and Latham (CL) which was based on the plastic work per unit volume expressed as follows [21]

$$D = \frac{W}{W_{cr}} = \frac{1}{W_{cr}} \int_0^{\varepsilon_f} \langle \sigma_1 \rangle \, d\varepsilon_{eq} \tag{5}$$

where W is the Cockcroft-Latham integral, σ_1 is the major principal stress, $\langle\sigma_1\rangle = \sigma_1$ when $\sigma_1 \geq 0$ and $\langle\sigma_1\rangle = 0$ when $\sigma_1 < 0$. The concept is that damage accumulates during straining until a critical value $W = W_{cr}$. As seen, the fracture depends on the stresses imposed as well as on the strains developed. Cockcroft and Latham have used the major principal stress over the equivalent plastic strain instead of the equivalent stress in order to account for the influence of the hydrostatic tension [21]. According to this model, the fracture cannot occur when there is no tensile stress operating, which implies that the effect of stress triaxiality on the failure strain is implicitly taken into account. Thus, W_{cr} remains fairly constant for varying temperature and strain rate. The CL one-parameter fracture criterion is of special interest in design, since it requires only one simple tensile test in order to determine the material constant W_{cr}.

In high velocity impact, shear stresses are mostly responsible for the formation and growth of through-thickness of crack [20, 22]. There is a bulk of evidence that ductile fracture may occur on a plane where the shear stress is maximum. The maximum shear stress criterion is expressed as

$$\tau_{\max} = \frac{1}{2} \max \{|\sigma_1 - \sigma_2|, |\sigma_2 - \sigma_3|, |\sigma_3 - \sigma_1|\} \tag{6}$$

where σ_1, σ_2 and σ_3 are principle stresses. The fracture is reached when $\tau_{\max}$ exceeds a critical value τ_{cr}. The MS failure criterion has been successfully applied in soil and rock mechanics and other geomaterials for decades [35, 36].

Due to simplicity, a constant effective plastic strain to fracture is also used to simulate crack formation and growth when the stress triaxiality varies spatially and temporally in a narrow range. Fracture is assumed to occur in a material element when the equivalent plastic strain ε_{eq} reaches a critical value ε_f

$$\varepsilon_p = \varepsilon_f \tag{7}$$

Rosenberg et al. [27] have used this failure criterion to follow the shearing process of steel plates by a flat-ended projectile. When the accumulated effective plastic strain ε_p of a given element in the simulation reaches the threshold value ε_f, its strength is reduced to zero at the subsequent time steps. According to their study, the plates bulging and plugging prediction were in excellent agreement with Woodward et al. [28] test data. There is an understanding that Eq. (7) is valid for all possible stress states. Even though the origin of this criterion goes back to the beginning of the 20$^{\text{th}}$ century, [34], it has found its way into almost all nonlinear commercial codes in 21$^{\text{st}}$ century. While this criterion lacks generally, practitioners like it because location of possible fracture site can be determined simply by constructing

colour-coded plots of the equivalent strain and data can be easily found in handbooks.

3. The materials

3.1. Armour plates

In this study, 30PM high-strength steel designed for armour vehicles were used for target plates. The material data obtained from laboratory tests are grouped in quasistatic and dynamic tests where the effects of large strain, strain rate hardening and stress triaxiality on strength and ductility of the material were studied independently of each other.

For the quasistatic tests, a high stability material testing machines MTS Criterion Model 45 and Instron 8862 equipped with optical 3D deformation analyzer were used to conduct various tensile and compression tests at five different strain rates ($\dot{\varepsilon}_0 = 10^{-4}, 10^{-3}, 10^{-2}, 10^{-1}$ and 10^{0} s^{-1}). All the specimens are taken from 10 mm thickness plates using a wire electrical discharge machine. For each strain-rate, three specimens are tested. For the quasistatic tensile tests, they have been performed at room temperature using both smooth and pre-notched axisymmetric specimens. Notched specimens with four different notched root radii were tested (R = 0.5 mm, R = 1.0 mm, R = = 2.0 mm and R = 4.0 mm). More details about the dimensions of specimens are presented in Fig. 1. The different notches introduce different levels of hydrostatic tension in the specimens during straining, which distinctly affect both the true stress and the strain to failure of the material. The initial radius of the gauge section was kept constant at 3 mm for all the specimens tested.

During the tests, applied load, the diameter reduction of the necking area crosshead displacement and longitudinal strain were measured. The optical 3D deformation analyzer apparatus has recorded the deformation rate and the diameter reduction in the cross-sectional area of the specimen during straining until the fracture (see Fig. 2). Therefore, true stress-strain curves were determined for each test. The number of parallels was three. This gave a total of 15 tests for smooth specimens at five different strain rates, and a total of 12 tests for notched specimens with different curvature radii at initial strain rate $\dot{\varepsilon}_0 = 10^{-4}$ s^{-1}.

The true stress and strain were calculated as:

$$\sigma = \frac{F}{A_s}, \quad \varepsilon = 2 \cdot \ln\left(\frac{d_0}{d}\right) \tag{8}$$

where F is the applied load, A_s is the current cross-sectional area, d_0 and d represent the initial and current diameter of the specimen.

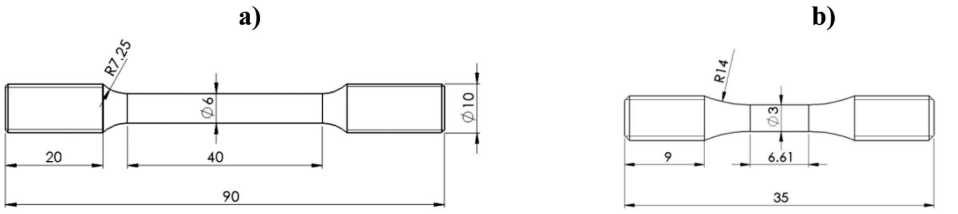

Smooth cylindrical specimen used in: a) quasistatic tests and b) dynamic tests

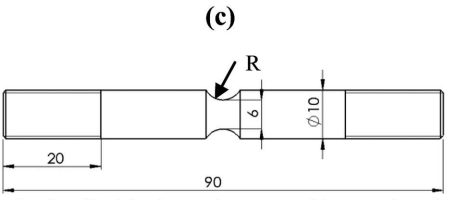

c) notched cylindrical specimen used in quasistatic test

Fig. 1. Geometries and dimensions (in mm) of smooth and pre-notched specimens used in material tests [24]

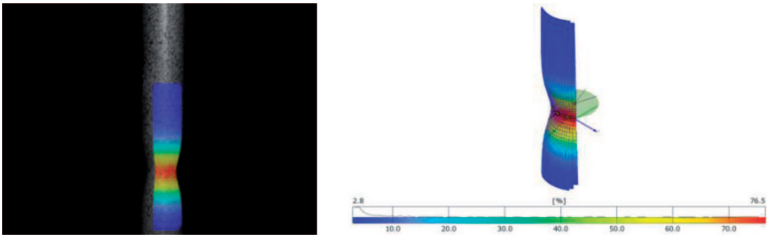

Fig. 2. True strain measurements during uniaxial tensile test using 3D deformation analysis

The yield stress parameter A and the hardening parameters B and n for the MJC constitutive relation in Eq. (1) were determined from the quasistatic tests performed on the smooth specimens at room temperature.

The measured longitudinal true stress σ_1 was further corrected for triaxiality effects, since this stress is not equal to the equivalent stress σ_{eq} after necking. The equivalent stress after necking was obtained using Bridgman's analysis [37]

$$\sigma_{eq} = \sigma_1 \Big/ \left(\left(1 + \frac{2R}{a}\right) \ln\left(1 + \frac{a}{2R}\right)\right) \tag{9}$$

where a is the specimen radius and R is the curvature radius of the current neck. The geometry of the neck is estimated using an empirical expression proposed by Le Roy et al. [38], where $a/R = 1.1\,(\varepsilon_{eq} - \varepsilon_U)$ for $\varepsilon_{eq} > \varepsilon_U$ and ε_U is the equivalent plastic strain at incipient necking. From the Bridgman-corrected true stress-strain curves, the MJC parameters A, B and n were determined by the best fit using the method of least squares available in

MatLab. Figure 3a shows a comparison between the experimental data and the calibrated MJC strain hardening model.

The stress triaxiality parameters D_1, D_2 and D_3 for the MJC failure strain relation in Eq. (3) were determined from the quasistatic tests performed on the smooth and pre-notched specimens. Figure 3b gives the measured true stress strain curves for both smooth and notched specimens based on the diameter reduction measurements. As seen, the stress is increased and the fracture strain is reduced with decreasing curvature radius, i.e. increased level of hydrostatic tension in the material during straining.

In order to determine the effect of multi-axial stress states on the strain to fracture, it is assumed that the stress triaxiality ratio $\sigma^* = \sigma_H \big/ \sigma_{eq}$ is constant for the tensile test and it is calculated as

$$\sigma^* = \frac{1}{3} + \ln\left(1 + \frac{a}{2R}\right) \tag{10}$$

where a is the initial radius of the specimen and R is the root radius of the notch [37]. The strain at fracture is determined as a function of the triaxiality ratio and the parameters D_1, D_2 and D_3 were determined by a best fit using the method of least squares (see Fig. 3c).

To determine the strain rate hardening parameter C for the MJC constitutive model and the parameter D_4 for the MJC failure strain, the quasistatic tensile tests were enhanced with dynamic tensile tests at higher strain rates (up to $\dot{\varepsilon} = 3 \times 10^3\ \mathrm{s}^{-1}$). Tests were performed on a modified Split Hopkinson Pressure Bar (SHPB) test setup. Smooth specimens with 3 mm gauge diameter were used. During the test, the diameter reduction of the specimen was measured until the fracture by the use of a high speed camera in order to determine the equivalent strain values. During tests, the equivalent stress at 4% of the equivalent plastic strain was collected at various deformation rates ranging from 10^{-4} to $3 \times 10^3\ \mathrm{s}^{-1}$ and a linear fit was established, as shown in Fig. 3d. In addition, the fracture strains were determined on that deformation rate range and a curve fit was established as shown in Fig. 3e. It is clearly seen that the 30PM steel provides low sensitivity to the variation of the deformation rate on the studied range.

Thermal softening parameter m is taken as unity considering a linear relation between the plastic flow and temperature rise.

This assumption seems to be reasonable for steel, and it was used in the Ref. [9], [24] and [26]. However, the temperature parameter D_5 in the MJC failure strain equation is taken equal to zero without performing any tests. The critical plastic work W_{cr} was determined by calculating the area under the true stress-strain curves. Since the major principle stress σ_1 varies over the cross-section after necking, the measured true stress represents its average value.

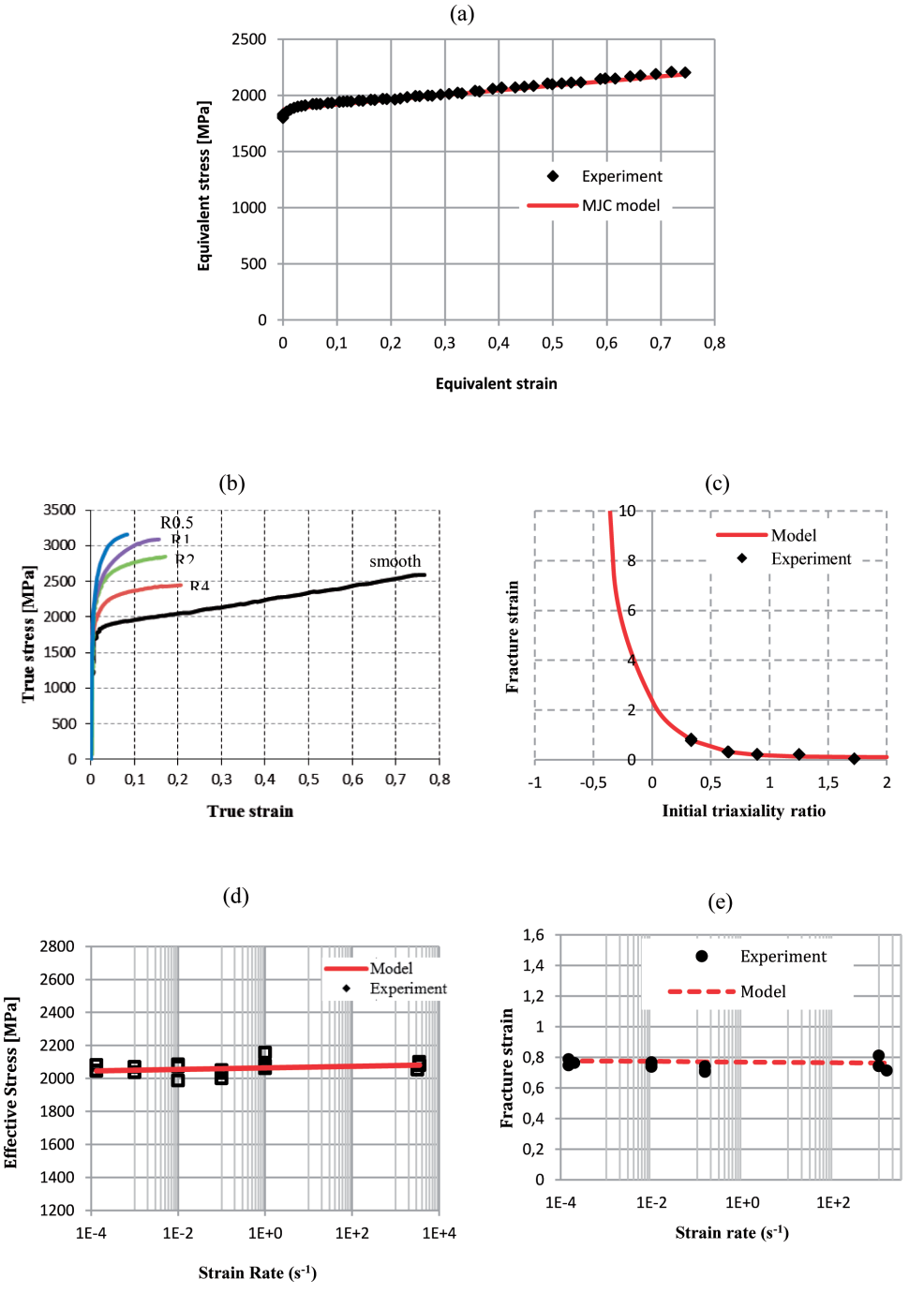

Fig. 3. Comparison between experimental data and model results for 30PM armour steel

The material constants for the MJC constitutive relation, the MJC failure strain and Cockcroft-Latham work for 30PM steel are given in Table 1 and Table 2. The constant plastic strain to failure was determined from equivalent stress-strain curves obtained from tensile tests on smooth specimens at room temperature. However, in this study, no shear test has been done. Preliminary numerical simulation of plate perforation indicates a maximum value of shear stress before failure equal to 1546 MPa. This value was used for one parameter fracture model based on the maximum shear stress.

Table 1.

MJC constitutive model parameters for target plates

Material	Hardness	Yield stress	Strain hardening			Strain rate hardening		Temperature softening
	HB	$\sigma_{0.2}$(MPa)	A(MPa)	B (MPa)	n	C	$\dot{\varepsilon}_0(s^{-1})$	m
30PM	488-566	1707	1875	415	0.98	0.001	2×10^{-4}	1.0

Table 2.

Material parameters for the fracture criteria obtained for the 30PM steel plates

Material	Modified Johnson-Cook (MJC)					Cockcroft-Latham (CL)	Maximum shear stress	Constant failure strain
	D_1	D_2	D_3	D_4	D_5	W_{cr} (MPa)	$\tau_{\max}$ (MPa)	ε_f
30PM	0.10	5.40	–2.66	–0.0012	0	1689	1546	0.752

3.2. Bullet projectile

In this study, 7.62×51 mm Armour Piercing ammunition, with protection level 3 according to Stanag 4569, is used in the ballistic impact tests. Schematic drawings and geometry of the ball bullet is given in Fig. 4.

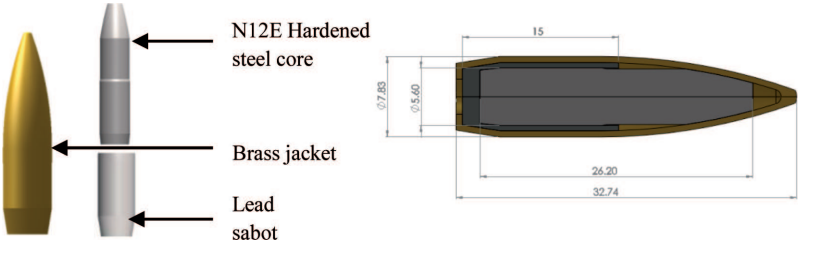

Fig. 4. Schematic drawing geometry of 7.62 mm AP bullet

A hard core projectile made of N12E steel with a small blunt section at the tip of the nose is inserted into a lead sabot, before the group is clamped onto a brass jacket. The total mass of the bullet is ~9.5 g with core mass of

~4.5 g. Material data for the bullet are generally not available in the open literature. Furthermore, it is not possible to make correct specimens from the bullet due to machining difficulties. Borvik et al. [9], Kilic et al. [11] and Buchar et al. [29] have reported some JC material constants for hard core projectile made of 1007 tool steel with 800 HV hardness which is designed for 7.62 mm NATO ball. Hardness investigation on the N12E hard steel core gave a value of 720 HV which was considered comparable to the 1007 steel core.

Table 3.

JC model parameters for 7.62 AP steel core

	Strain hardening			Strain rate hardening		m
	A (MPa)	B (MPa)	n	c	$\dot{\varepsilon}_0$ (s^{-1})	
Borvik et al. [9]	1200	50,000	1	0	5×10^{-4}	1
Kılıç et al. [11]	1900	1100	0.3	0.005	10^{-3}	1
Buchar et al. [29]	1650	807	0.1	0.008	–	1

Preliminary ballistics simulation studies with Ls-Dyna have shown that Kilic et al. [11] and Buchar et al. [29] material parameters (see Table 3) result in large plastic deformation on the bullet core after interaction with the armour plate, and the projectile residual velocity is underestimated. Borvik et al. [9] has modelled 7.62 AP bullet steel core as a rigid material. He used a yield strength of 1200 MPa but extremely high strain hardening parameters and without any strain rate hardening. Simulations have shown no projectile deformation but an overestimation of the penetration depth and projectile residual velocity. During the shot tests, the hardened steel core tip was shattered at early stage of the penetration process and the bullet core got a final cylindrical shape with blunt nose. Furthermore, the visual inspection of the bullet core after the impact showed a brittle fracture and no significant plastic deformation has been noticed on the bullet core (Fig. 5).

Fig. 5. 7.62 mm AP bullet core after shot tests

In this study, the Borvik et al. [9] bullet core constants are used to maintain its rigidity, however, an erosion criterion was added in order to describe the bullet erosion which affects the final results. A maximum effective

strain at failure $\varepsilon_f = 0.16$ was found to give comparable results. When the equivalent strain of a given element in the simulation reaches the threshold value (ε_f), its strength is reduced to zero at the subsequent time steps. This approach has been used also by Anderson et al. [12] to describe core erosion during impact and he assumed a constant failure strain $\varepsilon_f = 0.10$. Material constants of the brass jacket and the lead sabot for the MJC constitutive relation and CL failure criterion are given in Table 4 and Table 5.

Table 4.

Bullet jacket and core material constants for the MJC constitutive relation and CL failure criterion [9]

Material	Strain hardening			Strain rate hardening		m	CL
	A (MPa)	B (MPa)	n	c	$\dot{\varepsilon}_0$ (s^{-1})		W_{cr} (MPa)
Brass jacket	206	505	0.42	0.01	5×10^{-4}	1.68	914
Lead core	24	300	1.0	0.1	5×10^{-4}	1.0	175

Table 5.

General material constants for the MJC constitutive relation [10]

Material	E (MPa)	ν	ρ ($\frac{kg}{m^3}$)	C_p ($\frac{J}{kg}$K)	χ	α (k^{-1})	T_c^*
All steel alloys	210,000	0.33	7850	452	0.9	1.2×10^{-5}	0.9
Lead sabot	1000	0.42	10,660	124	0.9	2.9×10^{-5}	0.9
Brass jacket	115,000	0.31	8520	385	0.9	1.9×10^{-5}	0.9

4. Numerical models

All numerical simulations were carried out using the explicit finite element code LS-dyna. The projectile and the region in the target plate that undergoes large deformations were modeled using hexahedral constant stress solid element. Since the size of the impact region increased with oblique angle, a larger zone was required at large oblique zone. Geometries of the targets and bullet were similar to those used in the tests except the target was modelled somewhat smaller than in the test to save computational time. Rosenberg et al. [30] and Littlefield et al. [31] found that the diameter of plate should be at least 15 times larger than the projectile diameter in order to avoid lateral release effects. The target was also modelled as clamped along one boundary. The impact velocity was taken as 835 m/s. This value is average velocity based on large number of experimental tests. In addition, the element size of the bullet and the region of the targets which undergoes large deformation was $\Delta x = \Delta y = \Delta z = 0.2$ mm. The mesh is coursing from

the impact area to the outer edge of the plates. The mesh transition between regions is good enough to prevent stress wave reflections at the boundaries.

Exception for the plate impact area which subjected to large deformation and elements erosion, hybrid SPH/solid elements has been used. This approach allows the conversion of the high distorted solid elements to Smooth Particles Hydrodynamics. The generated particles keep the same mechanical properties and mass of the eroded elements. Figure 6 shows an example of typical modelling results where the AP projectile perforates a 3 mm thickness 30PM plate. The models are plotted as fringes of the equivalent stress.

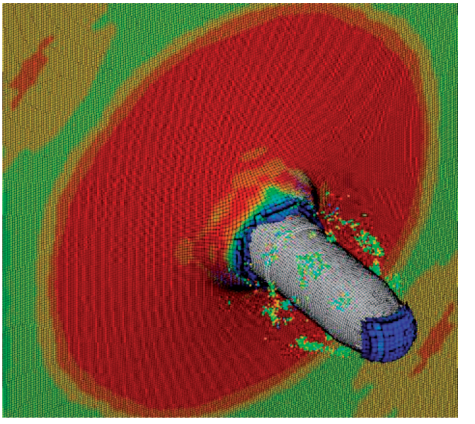

Fig. 6. A plot of typical perforation modelling using hybrid Solid/SPH elements

The constitutive behaviour of bullet and target materials was modeled using the MJC relation given by Eq. (1), while materials failure was modelled using different failure criteria. The MJC fracture criteria given by Eq. (4), the Cockcroft-Latham given by Eq. (5), the maximum shear stress given by Eq. (6), and the constant equivalent plastic strain fracture criteria were used for the target plates and the simulation results were compared. The bullet jacket and sabot material failure was modelled using CL, while the bullet core elements are eroded when their equivalent strain in the simulation reaches the threshold value.

Most simulations were run with material constants for the target based on MJC hardening constants determined from tensile tests, while some simulations were run with hardening parameters for the target based on compression tests. This was done to check of the possible effect of target thickness and compression strength on projectile penetration depth. Note that constants for compression tests give higher strength and strain hardening for the material than constants for tensile tests. For the bullet, element erosion was used to prevent overly distorted elements which reduce the time step towards zero and could cause error termination. The critical time step for element erosion was

taken equal to 5 ns. This approach sometimes eroded a few overly deformed elements in the pointed nose of the bullet jacket and hard core AP, but this is not expected to have any significant influence on the final results since the test results showed completely shattering of the bullet nose. Contact between the various parts was established using a penalty-based automatic_surface_to_surface algorithm. A segment-based penalty formulation was used in the stiffness option (Soft = 2) where the *dt* is updated only if the solution time step grows by more than 5%. This allows *dt* to remain constant in most cases, even if the solution time step slightly grows [15]. Control parameters are also used to control hourglass, termination of solution, times step size, contact and adaptive. One of the most important control tools in impact problems is time step scale factor. TSSF is used to provide optimum time step to confirm numerical stability. LS DYNA has default value of 0.9 but in this analysis 0.4 was chosen. FE simulations were conducted on a high performance compute cluster which consists of 20 CPU. In this study, no friction was assumed since many authors confirmed that at high velocity impact problems, the effect of friction is very low and it could be ignored [9, 10, 27].

Finally, although the impact velocity in this study is rather high, no additional EOS (which relates pressure, volume, and some thermal parameter, usually the internal energy or temperature) or artificial bulk viscosity was introduced in the simulations to treat possible shock waves. Thus, the relation between the pressure p and the volumetric strain ε_v is given by the linear expression $p = k\varepsilon_v$, where k is the bulk modulus. This seems appropriate for weak shocks [9]. According to Zukas et al. [1] and Meyers [33], only moderate pressures are generated for solid-solid impacts in the 0.5-2 km/s velocity regime, and non-linear EOS under such impact conditions to be of secondary importance.

5. Results and discussion

The ballistic tests were carried in the laboratory of ballistics at the Military University of Technology of Warsaw. Target Plates with 250×250 mm^2 and different thicknesses (3 mm, 6 mm and 8 mm) were mounted in a stiff frame and adjusted to the desired impact angle. Here, a maximum of 3 shots were performed in each target before it was replaced. A rifle was used to fire 7.62×51 mm AP ammunitions at velocity of 835±10 m/s. Note that seven shots were carried out for each plate configuration in order to provide an assessment of random scatter of the obtained experimental results.

During the tests, an optical velocity measuring system was available to measure the projectile initial velocity. In addition, a Phantom v12.1 high

speed camera was used in tests to record the penetration process and the projectile residual velocity.

High-speed camera images of perforation tests on 3 mm and 6 mm plates were compared with the numerical results at identical impact velocity using four failure criteria. Figure 7 shows bulging of the 3 mm plate after impact and the evidence for its tensile failure at the back surface. In addition, a small plug is formed and ejected.

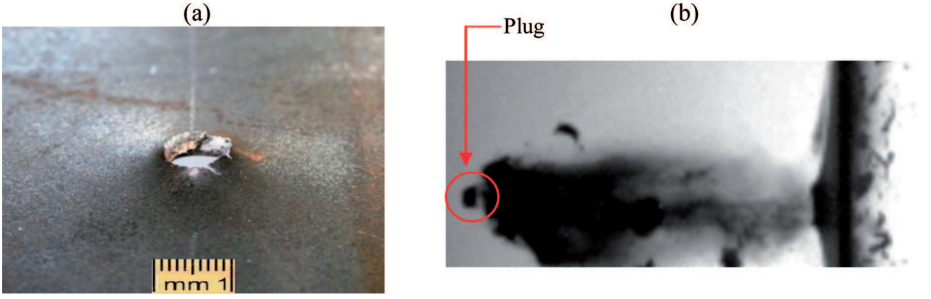

Fig. 7. a) 30PM plate hole after shot with 7.62 AP bullet, b) plate deformation during shooting

From the numerical simulations, it is seen that the plate bulging and deformation seems to be well described with the four fracture models (Fig. 8). However, the plugging mechanism couldn't be described by the maximum shear stress and the constant failure strain models. The MJC and CL fracture criteria have well predicted the small plug formation and gave similar plug shape.

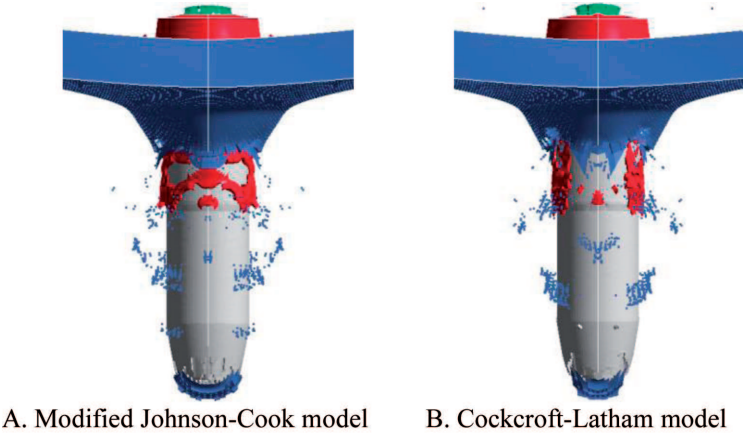

Fig. 8a. Failure patterns using different failure criteria (3 mm plate)

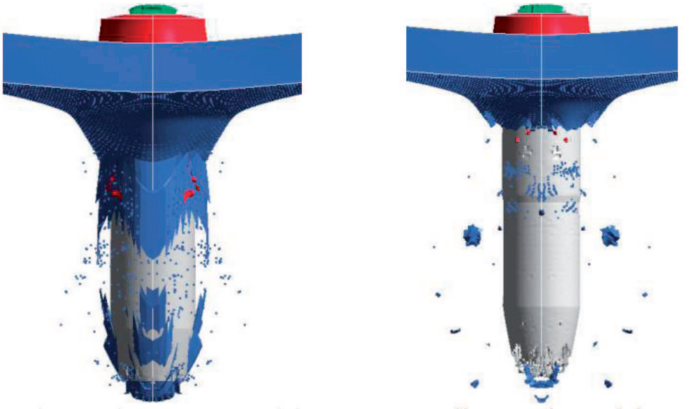

C. Maximum shear stress model D. Failure strain model

Fig.8b. Failure patterns using different failure criteria (3 mm plate)

The perforation tests on the 6 mm thickness plate showed that the plate was easily sheared by the high strains around the periphery of the projectile. Figure 9 shows the resulting shearing plugs after shots. A comparison with the numerical results showed an excellent prediction of the damage pattern by the MJC and CL fracture criteria (see Fig. 10). By the use of the maximum shear stress fracture criterion, the finite elements around the periphery of the projectile provided long elongation, and they took a ligament shape. This is physically and numerically unlike since the shear plugging develops in a narrow zone in the target followed by plug ejection. The constant failure strain model couldn't describe the shear plugging and only small fragments have been formed (Fig. 10).

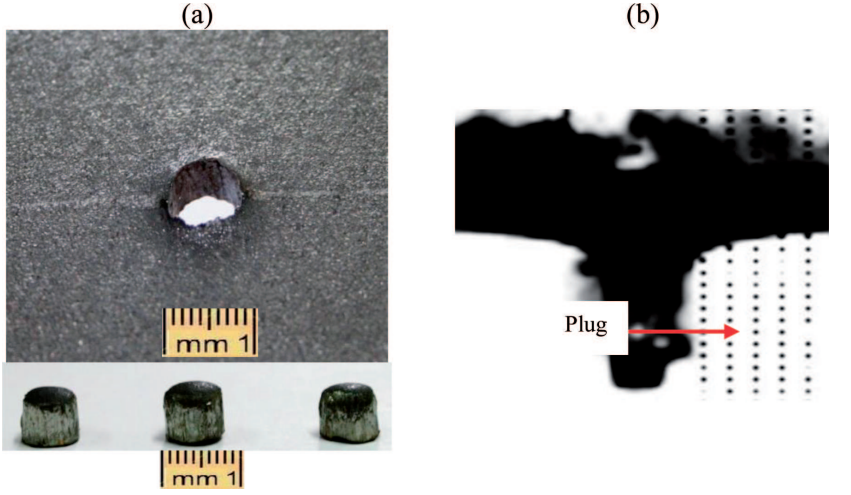

Fig. 9. a) Generated hole after shots of 6 mm 30PM steel plate. b) Resulting plugs after shots

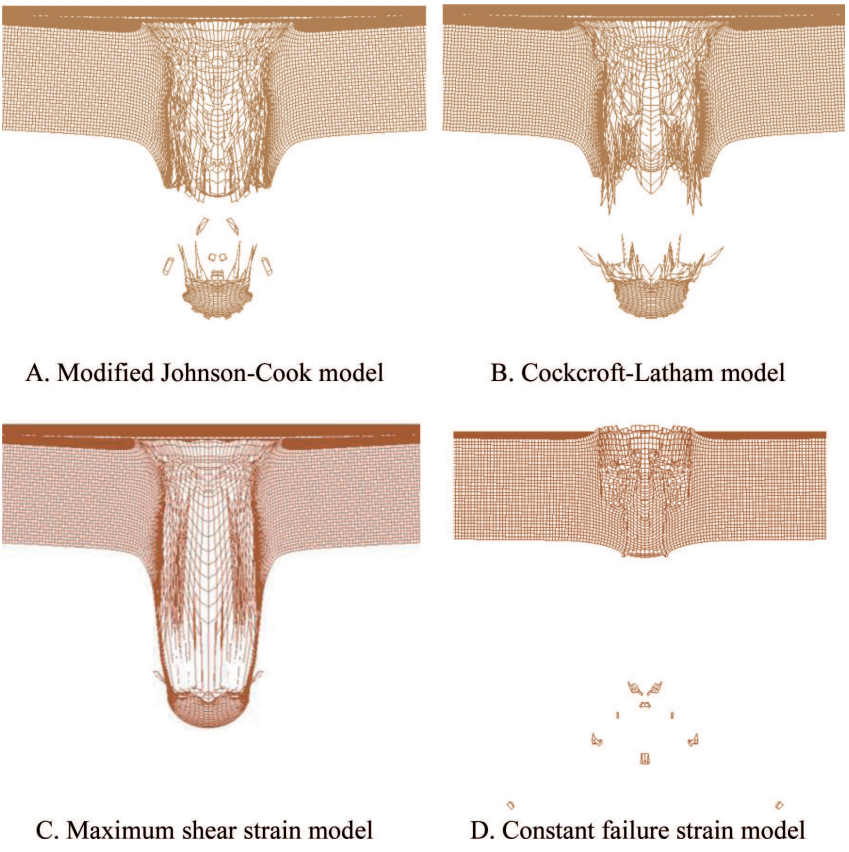

Fig. 10. Comparison between failure patterns of 6 mm plates modelled with different fracture criterion (the generated SPH particles are hidden to show clearly the hole and the ejected plug)

Figure 11 shows the projectile velocity history during the perforation of 3 mm and 6 mm thickness plates. Note that the experimental residual speed was measured by the use of high speed camera and movement analyzer software TemaMotion with ±15 m/s velocity measurement precision. The average residual speed was found to be 717 m/s and 406 m/s after the perforation of 3 mm plate and 6 mm plate successively. An excellent prediction of the projectile residual velocity was given by the MJC and CL fracture criteria for both plates with error estimation less than 2%. However, the maximum shear stress model has underestimated the projectile residual velocity by 2% and 24% after perforation of 3 mm and 6 mm plates. Thus, the projectile residual velocity was overestimated by 3% and 27% for the 3 mm and 6 mm plate by the use of constant failure strain model.

The reason why the maximum shear stress and the constant failure strain fracture criteria could not describe correctly the failure pattern is believed to be that they cannot predict the stress triaxiality as well as the MJC and

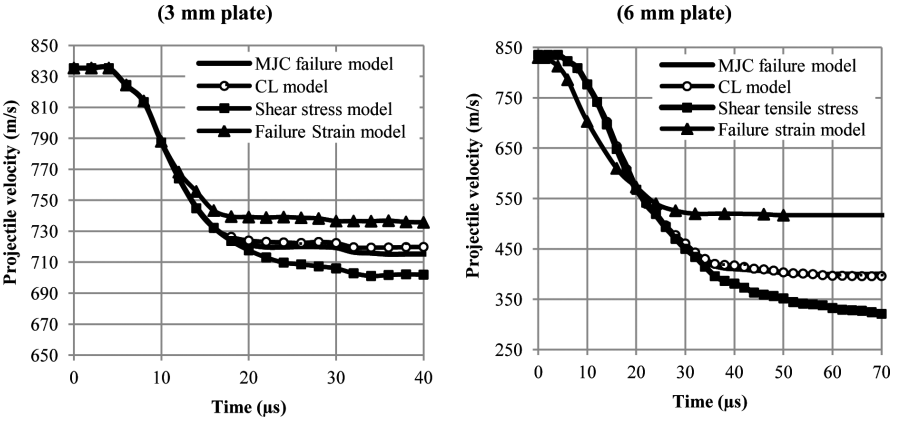

Fig. 11. Projectile velocity history during perforation of 30PM steel plates

CL fracture criteria. The comparisons indicate also that the MJC fracture criterion based on the stress triaxiality and strain rate effects, and the one parameter CL fracture criterion based on the plastic work where the effect of stress triaxiality on the failure strain is implicitly taken into account, seem to give equally good results. Thus, the CL fracture criterion is shown to be promising for this type of problems, when taking its simple calibration into account. This is important for an armour designer, since it is required that the number of material constants in numerical simulations should be minimized. Also, the numerical simulations showed that for these steel plates the triaxiality stress effect becomes more important than the strain rate effect.

In order to determine the limiting thickness of the 30PM plates at 835 m/s impact velocity, additional perforation tests were performed on 8 mm plates. Figure 12a shows a cross-sectional view of the resulting crater. Despite the fact that the 6 mm plates were fully perforated by the 7.62 AP bullets,

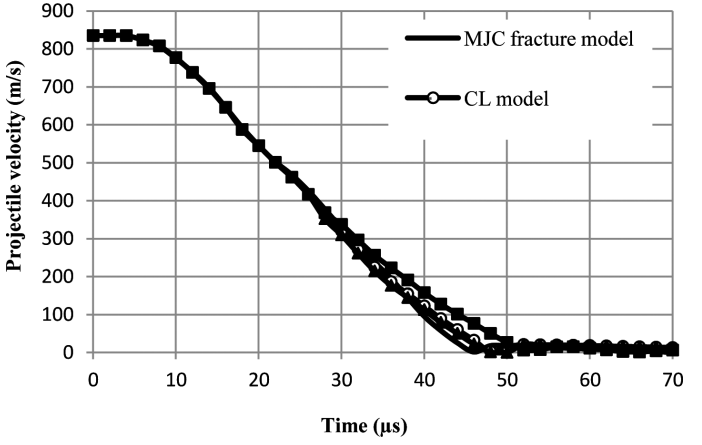

Fig. 12. Projectile velocity history during perforation of 8 mm thickness 30PM steel plates

the 8 mm plates could stop the projectile and a measured crater depth of 2.20 mm has been obtained with smooth plate bulging. Anderson et al. [32] has experienced similar issue in studying the minimal plate thickness which needs to stop steel rods at a given velocity. As expected, the limiting thicknesses of these plates are greater than the corresponding penetration depths into semi-infinite targets.

The numerical simulations have predicted the projectile stop at a time of 45-50 μs, independent on the chosen fracture criteria (see Fig. 12). However, the results about the penetration depth were disappointing, since they were overestimated for the four fracture criteria described above (Fig. 13b).

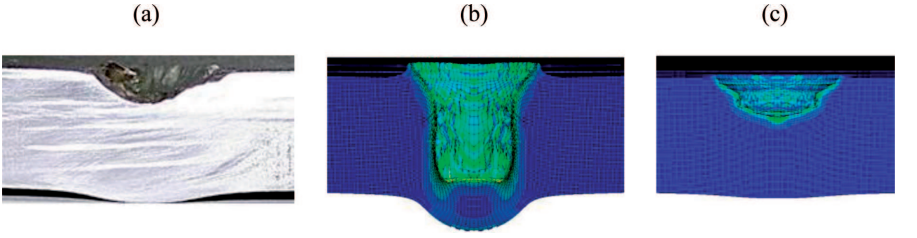

Fig. 13. Comparison between experimental and numerical penetration depth of 8 mm 30PM plates impacted by 7.62 AP bullet: (a) experiment result, (b) MJC strain hardening parameters determined from tensile tests; (c) MJC strain hardening parameters determined from compression tests

A reason which could influence modelling results is that the MJC strength model was calibrated under tensile test conditions, while the penetration of 8 mm thickness plates is highly subjected to material compression instead of material tension. Therefore, by introducing high material strength slope, the resistance to bullet penetration may increase. Therefore, uniaxial compression tests were performed where cylindrical specimen with length to diameter ratio of 1.0 made of 30PM steel was used. A silicon lubricant was used to reduce contact friction between specimen interfaces and compression plates.

After the determination of equivalent stress-strain curve (see Fig. 14), the obtained hardening parameters of the MJC constitutive relation was found to be A = 1720 MPa, B = 2106 MPa and n = 0.63. It is clearly seen that 30PM steel provides a higher compressive strength due to the large strain hardening in compressive loading. These parameters were used in the numerical simulations of penetration of the 8 mm plates. The predicted penetration depths were in accordance with the experimental results (Fig. 13c).

In simulations, the depth of the crater was found to be 2.6 mm for the 8 mm plate. This value is very comparable with the experimentally measured depth of 2.2 mm. The slight difference is believed to be because of the

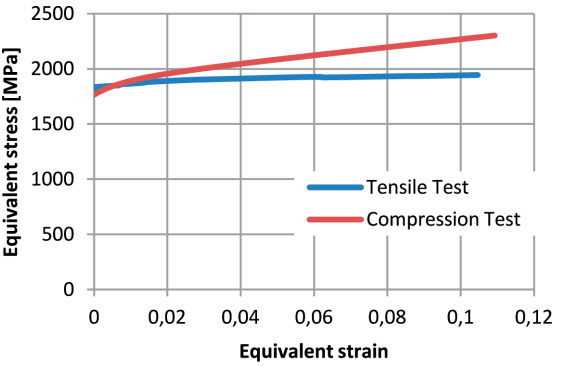

Fig. 14. Comparison between tensile and compression stress-strain curves of 30PM steel

stochastic nature of ballistics. In addition to the initial yaw of bullets, they will not cause a perpendicular penetration, but with an angle of obliquity.

6. Concluding remarks

This paper presents a numerical investigation of fracture criterion influence on perforation of high-strength steel plates made of 30PM steel subjected to 7.62×51 mm AP projectile. An evaluation of four ductile fracture models was performed to identify the most suitable fracture criterion. Included in the paper are the Modified Johnson-Cook (MJC) constitutive model coupled separately with MJC failure model, the Cockcroft-Latham (CL), the maximum shear stress or the constant failure strain models. A 3D explicit Lagrangian algorithm that includes both elements and particles is used in this study to automatically convert distorted elements into meshless particles during the course of the computation. Numerical simulations are examined by comparing with the experimental results. According to numerical and experimental data developed during the study, the following main conclusions can be drawn:

- The Modified Johnson-Cook constitutive model together with MJC fracture model, which is formulated in the space of the stress triaxiality and the equivalent plastic strain to fracture found capable of predicting the realistic fracture patterns and at the same time the correct projectile residual velocities.
- This study has shown that Cockcroft and Latham one parameter fracture criterion where only one simple material test is required for calibration is found to give good results and able to predict the shear band failure and the projectile residual velocity at different plate thicknesses.
- The maximum shear stress fracture criterion fails to capture the shear

plugging failure and material fracture properties cannot be fully characterized with the constant fracture strain.

- This study showed also that the 3D Finite Elements algorithm with Hybrid solid/SPH elements is capable to predict the armour steel plate deformation and failure behaviour when it is subjected to armour piercing projectile at high velocity impact.

Acknowledgments

The authors would like to thank the Military Polytechnic School of Algiers and Institute of Armament – Military University of Technology – of Poland for the financial and technical support. Furthermore, the authors would like to acknowledge Prof. Jacek Janiszewski, Dr. Zbigniew Surma, Dr. Michał Grązka and M.Sc. Marcin Sarzyński for the material test program carried out and the ballistic tests.

Manuscript received by Editorial Board, July 04, 2014;
final version, May 12, 2015.

REFERENCES

[1] Zukas J.A., Nicholas T., Swift H.F., Greszczuk L.B., Curan D.R.: Impact dynamics. John-Wiley and Sons, Inc., New York, 1982.
[2] Johnson G.R., Cook W.H.: Fracture characteristics of three metals subjected to various strains, strain rates, temperatures and pressures. Engineering Fracture Mechanics 1985; 21: 31-48.
[3] Johnson G.R., Cook W.H.: A constitutive model and data for metals subjected to large strains, high strain rates and high temperatures. In: Proceedings of seventh international symposium on ballistics, Netherlands, 1983.
[4] Zukas J.A.: High velocity impact dynamics. John-Wiley and Sons, Inc., New York, 1990.
[5] Zukas J.A.: Introduction to hydrocodes. Computational Mechanics Associates. Baltimore 2004.
[6] Rajendran A.M.: Advanced numerical simulation of failure in solids under blast and ballistic loading: A review. In; Shukla A et al. (Eds.) Dynamic failure of materials and structures, springer, New York, 2010; 336-347.
[7] Mehra V., Sijiy C.D., Mishra V., Chaturvedi S.: Tensile instability and artificial stresses in impact problems in SPH. J Physics 2012; 377: 102-112.
[8] Dey S., Borvik T., Hopperstad O.S., Langseth M.: On the influence of the fracture criterion in projectile impact of steel plates. Computational materials Science 2006; 38: 176-191.
[9] Borvik T., Dey S., Clause A.H.: Perforation resistance of five different high-strength steel plates subjected to small-arms projectiles. Int J Impact Engineering 2009; 36: 948-964.
[10] Borvik T., Olovsson L., Dey S., Langseth M.: Normal and Oblique impact of small arms bullets on AA6082-T4 aluminum protective plates. Int J Impact Eng 2011; 38: 577-589.
[11] Kılıç N., Ekici B.: Ballistic resistance of high hardness armor steels against 7.62 mm armor piercing projectile. Materials and Design 2013; 44: 35-48.
[12] Andersen Jr. C.E., Burkins M.S., Walker J.D., Gooch W.A.: Time-resolved penetration of B4C tiles by the APM2 bullet. Computer Modeling in Engineering & Sciences 2005; 8(2): 91-104.

[13] Monaghan J.J.: SPH without a tensile instability. J Computational Physics 2000; 159: 290-311.
[14] Abaqus theory manual, 2014.
[15] Ls-Dyna theory manual. Livermore Software Technology Corporation (LSTC); 2014.
[16] Beal T., Van Dorsselaer N., Lapoujade V.: A contribution to validation of SPH new features. 9th European Ls-Dyna Conference 213, France.
[17] Woodward R.L.: Material failure at high strain rates. In; Zukas JA (Ed) High velocity impact dynamics. John-Wiley and Sons, Inc., New York, 1990; 65-126.
[18] Anderson T.L.: Fracture Mechanics (Fundamentals and Applications). CRC Press, Inc. 1991.
[19] Anvari M., Liu J., Thaulow C.: Dynamic ductile fracture in aluminum round bars: experiments and simulations. Int J Fracture 2007; 143: 317-332.
[20] Hancock J.W., Meckenzie A.C.: On the mechanisms of ductile failure in high strength steels subjected to multi-axial stress-states, Journal of the Mechanics and Physics of Solids, Vol. 24, pp. 147-169, 1976.
[21] Cockcroft M.G., Latham D.J.: Ductility and workability of metals. Journal of the Institute of Metals 1968; 96: 33-39.
[22] Wierzbicki T., Bao Y., Lee Y.W., Bai Y.: Calibration and evaluation of seven fracture models. Int J Mechanical Sciences 2005; 47: 719-743.
[23] Woodward R.L.: A structural model for thin plate perforation by normal impact of blunt projectiles. Int J Impact Eng 1987; 6: 128-140.
[24] Borvik T., Hopperstad O.S., Berstad T., Langseth M.: A computational model of viscoplasticity and ductile damage for impact and penetration. European Journal of Mechanics 2001; 20: 685-712.
[25] Bao Y., Wierzbicki T.: A comparative study on various ductile crack formation criteria. J Eng Materials and Technology 2004; 126: 314-324.
[26] Skoglund P., Nilsson M., Tjernberg A.: Fracture modeling of a high performance armour steel. J Phys IV France 2006; 134: 197-202.
[27] Rosenberg Z., Dekel E.: Terminal ballistics. Springer, New York, 2012.
[28] Woodward R.L.: Material failure at high strain rates. In; Zukas JA (Ed) High velocity impact dynamics. John-Wiley and Sons, Inc., New York, 1990; 65-126.
[29] Buchar J., Voldrich J., Rolc S., Lisy J.: Ballistic performance of dual hardness armor. In: 20th International symposium on Ballistics Orlando, September 2002; 23-27.
[30] Rosenberg Z., Dekel E.: How large should semi-infinite targets be? Proceedings of the 45th meeting of the aeroballistics range association, Huntsville, Alabama, 10-14 Oct 1994.
[31] Littlefield D.L., Anderson C.E., Partom Y., Bless S.J.: The penetration of steel targets finite in radial extent. Int J Impact Eng 1997; 19: 49-62.
[32] Anderson C.E., Morris B.L., Littlefield D.L.: Penetration mechanics database. SwRI Report 3593/001. Southwest Research Institute,1992, TX.
[33] Meyers M.A.: Dynamic behavior of materials. New York, John Wiley and Sons, 1994.
[34] Huber M.T.: Contribution to the foundation of the strength of the material (in Polish, translated to English by Professor. M. Zyczkowski in connection with the M.T. Huber Century Symposium, Krakow, August, 2004). Czasopismo Techniczne, Lwow 1904; 22: 81.
[35] Bardet J.P.: Lode dependences for isotropic pressure-sensitive elastoplastic materials. Transactions of the ASME 1990; 57: 498-506.
[36] Bigoni D., Piccolroza A.: A new yield function for geomaterials. In: Viggiani C, editor. Constitutive modelling and analysis of boundary value problems in geotechnical engineering, Napoli; 22-24 April 2003; 266-81.
[37] Bridgman P.W.: Studies in Large Plastic Flow and Fracture. McGraw-Hill, New York. 1952.
[38] Le Roy G., Embudy J.D., Ashly M.F.: A model of ductile fracture based on the nucleation and growth of voids. Acta Mettalurgica 1981; 29: 1509-22.

Wpływ kryterium pękania materiału na perforację płyt ze stali pancernej pociskiem przeciwpancernym

S t r e s z c z e n i e

Artykuł przedstawia numeryczne badania wpływu kryterium pękania materiału na perforację płyt ze stali pancernej 30PM pociskiem przeciwpancernym 7,62×51 mm. Dokonano oceny czterech modeli pękania materiałów plastycznych w celu wyboru najbardziej odpowiedniego z nich. W artykule wykorzystano zmodyfikowany model konstytutywny Johnsona-Cooka (MJC) sprzężony z jednym czterech kryteriów pękania: kryterium MJC, kryterium Cockrofta-Lathama (CL), kryterium maksymalnego naprężenia stycznego i kryterium stałego granicznego odkształcenia. Zastosowano trójwymiarowy algorytm w opisie Lagrange'a, zawierający zarówno skończone elementy jak i cząstki, z automatyczną konwersją zniekształconych elementów w bezsiatkowe cząstki. Wyniki symulacji numerycznej oceniono na postawie porównania z wynikami doświadczeń. Model pękania MJC, sformułowany w przestrzeni trójosiowości naprężenia i równoważnego odkształcenia plastycznego, pozwolił przewidzieć realistycznie obraz pękania materiału i wartości prędkości resztkowych pocisków. Jednakże wyniki badań wykazały, że również jednoparametrowy model CL, dla którego kalibracji wystarczy jeden prosty test materiałowy, daje porównywalne wyniki z kryterium MJC. Stwierdzono, że kryterium maksymalnego naprężenia stycznego niepoprawnie opisuje proces tworzenia się korka. Również kryterium stałej wartości odkształcenia granicznego nie może być użyte do scharakteryzowania procesu niszczenia materiału.